Catalysis Today 390-391 (2022) 316–325

Contents lists available at ScienceDirect

Catalysis Today

journal homepage: www.elsevier.com/locate/cattod

The effect of non-ionic surfactants on the sustainable synthesis of selected MOFs

Nejat Redwan Habib [a,b], Raquel Sainz [a], Abi M. Taddesse [b], Isabel Diaz [a,*]

[a] Instituto de Catálisis y Petroleoquímica, CSIC, c/Marie Curie 2, 28049 Madrid, Spain
[b] Department of Chemistry, Haramaya University, Haramaya, Ethiopia

ARTICLE INFO

Keywords:
Sustainable MOF
Non-ionic surfactants
Crystal growth
NH_2-MIL-53(Al)
MIL-100(Fe)
UiO-66

ABSTRACT

The MOFs selected in this work are NH_2-MIL-53(Al), MIL-100(Fe) and UiO-66 type (Zr-BDC and NH_2-Zr-BDC). We have tried to assist the sustainable synthesis of MOFs, at room temperature and in water as a solvent, with the presence of non-ionic surfactants: Pluronic F127 and P123. The parent MOFs prepared at room temperature with water solvent commonly grow in the form of agglomerates of small crystallites in all cases. The X ray diffraction patterns of surfactant templated NH_2-MIL-53(Al) with F127 and MIL-100(Fe) with F127 and P123 show some differences in peak intensity indicating preferential crystal growth along one direction. This effect was confirmed by scanning and transmission electron microscopy, yielding long shaped crystals with more or less uniform morphology, notably larger than the parent MOFs. In the case of UiO-66 type (Zr-BDC and NH_2-Zr-BDC) MOFs, the X ray diffraction profiles of the parent and the surfactant templated MOFs do not show noticeable difference, which might be due to the semi-amorphous nature of these MOFs. However, the scanning and transmission electron microscopy images show larger particles in surfactant templated UiO-66 type Zr-MOFs compared to their parent counterparts.

1. Introduction

Metal organic frameworks (MOFs) are formed by combination of organic ligands with metal ions or clusters [1]. MOFs possess voids due to the particular condensation of organic ligands and have special features such as modular structure and very high specific surface area which vary depending on the MOF types [2]. The availability of various metal ions and organic ligands facilitates the design and synthesis to form different types of MOFs with different shapes [3,4] for intended applications such as biomedicine and phototherapy [5,6], sensing [7], adsorption [8] or catalysis [9]. However, the environmental impact and high economic cost of the synthesis of MOFs seems to be hindering their scalability to reach industrial applications. Ibarra et al., used near critical water (300 °C) as cleaner option to synthesize microporous MOF. The authors stated that, when water approaches near to critical point (374 °C, 220 bar) its dielectric constant decreases and acts as typical non-polar solvent. This enables the water to solubilize the organic ligand of the MOF precursor as an alternative of the organic solvent used in convectional synthesis [10]. Sustainable synthesis of MOFs at room temperature with water as a solvent by using linker salts could be a solution to ease the environmental problems as well the cost associated with energy demands [11–15]. Room temperature synthesis of MOFs implies precipitation methods that usually convey in the formation of nanocrystalline aggregated small crystals or small domains of MOFs which are difficult to characterize and therefore to identify and understand, eventually making the design of these materials less amenable.

Surfactants have crossed paths in the synthesis of MOFs aiming to assist their porous structures in the same manner as in zeolites [16]. Surfactants are amphiphilic molecules that form micelles which in particular conditions pack forming self-assembled crystal structures, this capacity has turn them into excellent templates in the synthesis of Ordered Mesoporous Materials (OMM) [17]. Following this templating mechanism of surfactants in OMMs, the idea was applied in MOFs aiming to create hierarchical porosity [18,19]. For example, Seoane et al., synthesized Al trimesate MOFs in the presence of cationic surfactant hexadecyltrimethylammonium bromide (CTAB) at 120 °C in water/ethanol as solvent. Depending on the pH and solvent ratio, MIL-96, MIL-100 and MIL-110 MOFs was obtained. The MIL-100 synthesized displayed microporosity of the Al-MOF framework and non-ordered inter-crystallite mesoporosity due to the presence of CTAB [20]. Similar results were obtained in our laboratory when we used CTAB in the room temperature synthesis of NH_2-MIL-53(Al) in water.

* Corresponding author.
E-mail address: idiaz@icp.csic.es (I. Diaz).

https://doi.org/10.1016/j.cattod.2021.09.028
Received 22 July 2021; Received in revised form 29 August 2021; Accepted 23 September 2021
Available online 29 September 2021

Mesoporosity was formed by entrapped CTAB while the MOF precipitated in the form of nanoparticle aggregates [21]. Recently, Li et al., created microporous crystals with mesoporous channels using amphoteric surfactant cocamidopropyl betaine (CAPB) on NH_2-UiO-66(Zr) MOF at 60 °C with formic acid modulator and water as a solvent [22]. The same surfactant was also employed by Giles et al., in the synthesis of HKUST-1. The surfactant induced wheat sheaf-shaped crystalline morphology different than the usual needle like HKUST-1 morphology as a result of the surfactant monomer interaction with the MOF during crystal growth [23]. Zhang et al., synthesized hierarchical MOF by templating Cu-BTC with anionic surfactant sodium benzenesulfonate (SBS). Cu and Zn hydroxy double salt used as metal precursor, in organic solvent at room temperature yielded super-fast crystal nucleation [24]. The effect of ionic surfactants on the formation of hierarchical MOFs has been beautifully addressed by Li et al. [25]. Accordingly, the hierarchical porosity can be induced in MOFs through strong interactions of the surfactant micelles with the MOF precursor resulting in uniform ordered hierarchical porosity as shown by Zhang et al. [24]. Yet, there is the other possibility, when surfactant micelles interact weakly with the MOF precursor and end up entrapped in agglomerated small particle-MOF yielding random intercrystalline hierarchical porosity [21].

Furthermore, the role of surfactants in the control of crystal growth of MOFs has been fully exploited with the use of non-ionic surfactants. These block-copolymer surfactants are built up from long chains of polyethylene oxide (EO)x and poly-propylene oxide (PO)y that in acidic conditions may form micelles leading to soft templating, whereas at milder pHs seem to act as surface crystal growth controllers [25]. Non-ionic surfactants such as Pluronic F127 ($EO_{106}PO_{70}EO_{106}$) have been reported to affect crystal size, morphology and surface properties of MOFs instead of templating mesoporosity. This effect has been mostly reported either using organic solvents or high temperature or both in the synthesis of MOF. Falcaro et al., synthesized MOF-5 in the presence of F127 by solvothermal method forming iso-direction microscopic superstructure called it Desert Rose Micropartciles (DRMs). These formed DRMs particles created an ideal effect on MOF-5 morphology and increased crystal growth by factor of 3 compared to the convectional solvothermal synthesized MOF-5 [26]. Interestingly F127 has also been employed to create single crystal of Cu-BTC in ethanol and water medium. The F127 surpasses the formation of fast porous Cu-BTC by inhibiting the contact between the salt solutions and the ligand, resulting in large Cu-BTC single crystals grown along the a-axis [27]. Cheng et al., prepared surfactant free large crystal of NH_2-MIL-53(Al) by using DMF-water mixed solvent at 150 °C. Increasing amount of water in the mixture of solvents created large crystals with different morphology than the convectional with DMF solvent only synthesized NH_2-MIL-53 (Al) [28]. MIL-100(Fe) particle size and morphology were modulated by changing the metal precursor valence state of the MOF in hydrothermal conditions in surfactant free system. In the experiment, ferric and ferrous sulfate with different molar ratios in the presence of hydrofluoric acid (HF) were used to bring the desired change [29]. For UiO-66 structure type MOFs, size and morphology controlled synthesis has been researched by using acetic acid and hydrofluoric acid as crystal and shape modulator [30,31]. In the above syntheses techniques, the methods involve high temperature and organic solvent or mixture of organic solvent and water or either of those in the presence of surfactant.

In our previous work, we have been focusing on sustainable synthesis of MOFs at room temperature with emphasis on the use of water as a solvent. The common morphology in these sustainable syntheses is the formation of aggregates of very small crystallites (5–10 nm) as a result of the rapid precipitation of the MOF phase. In this particular work, we employed non-ionic surfactants Pluronic F127 and P123 to survey the effect in the crystal growth and shape during the synthesis of MOFs of interest in heterogeneous catalysis such as NH_2-MIL-53(Al), MIL-100 (Fe) and UiO-66 type MOFs (Zr-BDC and NH_2-Zr-BDC). MIL-53(Al) MOF has breathing effect in which the ability of modifying shape and size of cavities depend on the guest specifically located in the pores [32]. Amino functionalized MIL-53(Al) has further broadened the catalytic activity of these types of MOFs being the amino group active centers in catalytic reactions [32–34]. The mesoporous MIL-100(Fe) is very attractive candidate for catalysis due to the mesoporous cavities, metal centers with Lewis acid and redox properties, non-toxic behavior and low cost [14]. UiO-66 type Zr-BDC and NH_2-Zr-BDC MOFs are good candidates in catalysis due to their large window size which facilitates diffusion of reactants and products [35]. Besides that, the strong interactions of the metal in tetravalent oxidation state with the carboxylate ligand makes these types of MOFs very stable during catalytic reactions [36].

2. Experimental section

2.1. Synthesis of NH_2-MIL-53 (Al)

NH_2-MIL-53(Al) was prepared according to published approach with the addition of Pluronic F127 surfactant [13]. In the typical synthesis, 6 mmol of $AlCl_3{\cdot}6H_2O$ (Sigma -Aldrich, 99%) are dissolved in 3 mL of H_2O (solution 1) and 6 mmol of 2-amino terephthalic acid (NH_2-H_2BDC (Sigma -Aldrich, 99%) in 13.05 mL 1 M NaOH (Solution 2). NaOH was used to deprotonate the carboxylic groups of the organic linker. Slight excess volume of NaOH was used to fully deprotonate the NH_2-H_2BDC linker the stoichiometrically calculated amount of which was 12 mL. Pluronic F127 (Sigma-Aldrich) with molar ratios (0.005, 0.01 and 0.025) calculated as surfactant/metal salt mole ratios were added for surfactant templated synthesis in solution 2 after the linker is fully dissolved. Solution 1 was added to solution 2 under stirring after forming clear solutions in both cases which resulted instantaneous yellow precipitates. The reaction was left under slow stirring for 24 h at room temperature. After 24 h, the precipitate formed was washed with H_2O (3x) and ethanol (2x) then dried at room temperature. The sample synthesized without surfactant is labeled as A0 and the samples synthesized with F127 surfactant using 0.005, 0.01 and 0.025 F127/$AlCl_3{\cdot}6H_2O$ molar ratios are labeled as AF0.005, AF0.01 and AF0.025, respectively.

2.2. Synthesis of MIL-100(Fe)

MIL-100(Fe) was prepared according to published approach including the addition of F127 and P123 surfactants [14]. Solution 1 was prepared by adding 7.6 mmol of trimesic acid (H_3BTC, Across Organics, 98%) in 23.72 mL of 1 M NaOH and solution 2 was prepared by adding 11.4 mmol of $FeCl_2{\cdot}4H_2O$ (Across Organics, 99 +) in 97.2 g of H_2O. Pluronic F127 and P123 (Sigma-Aldrich) with molar ratios (0.01, 0.05 and 0.1) calculated as surfactant/metal salt molar ratios were added for surfactant templated synthesis in solution 2 in separate synthesis for each surfactant. After formation of clear solutions in each case, solution 1 was added to solution 2 under stirring which brings green suspensions. After 6 h, it started forming brown precipitates. After 24 h under room temperature, the resulting precipitates was washed with H_2O (3x) and ethanol (2x) followed by drying under room temperature. The sample synthesized without surfactant is labeled as F0 and the sample synthesized with F127 surfactant using 0.01, 0.05 and 0.1 F127/ $FeCl_2{\cdot}4H_2O$ molar ratios are labeled as FF0.01, FF0.05 and FF0.1, respectively. Samples prepared with P123 surfactant using 0.01, 0.05 and 0.1 P123/$FeCl_2{\cdot}4H_2O$ molar ratios are labeled as FP0.01, FP0.05 and FP0.1, respectively.

2.3. Synthesis of UiO-66 type MOFs (Zr-BDC and NH_2-Zr-BDC)

For the synthesis of UiO-66 type Zr-MOF, we used the linker salt approach modified with surfactants [13,14,37]. For Zr-BDC, 6.05 mmol of $ZrOCl_2{\cdot}8H_2O$ (Sigma-Aldrich, 98%) in 28 mL H_2O (solution 1) and 6.2 mmol of H_2BDC (Across Organics, 99 + %) (for NH_2-Zr-BDC

synthesis NH_2-H_2BDC) (Sigma -Aldrich, 99%) in 22 mL H_2O (solution 2) were dissolved separately. The two solutions were stirred for 30 min independently. 14.5 mL 1 M NaOH was added in solution 2 (F127 and P123 with molar ratios 0.01, 0.05 and 0.1) calculated as surfactant/-metal salt mole ratios for surfactant templated synthesis for each surfactant after the linker was fully dissolved. After clear solutions are formed in each case, solution 1 was added to solution 2 slowly under room temperature which led to instantaneous white precipitates for Zr-BDC and yellow precipitates for NH_2-Zr-BDC. After 24 h, the precipitate formed was washed with H_2O (3x) and ethanol (2x) then soaked for 5 days with acetone, changing to fresh one daily. Finally, the samples were dried at room temperature. Zr-BDC and NH_2-Zr-BDC synthesized without surfactant are labeled as Z0 and N0 respectively, Zr-BDC and NH_2-Zr-BDC synthesized in the presence of F127 surfactant with 0.01, 0.05 and 0.1 F127/$ZrOCl_2{\cdot}8H_2O$ molar ratios are labeled ZF0.01, ZF0.05 and ZF0.1 and NF0.01, NF0.05 and NF0.1, respectively. Zr-BDC and NH_2-Zr-BDC synthesized in the presence of P123 surfactant with 0.01, 0.05 and 0.1 P123/$ZrOCl_2{\cdot}8H_2O$ molar ratios are labeled as ZP0.01, ZP0.05 and ZP0.1 and NP0.01, NP0.05 and NP0.1, respectively.

2.4. Characterization techniques

Mesoscopic order was studied by low angle X-Ray Diffraction (XRD). Besides, high angle diffraction was employed to determine the crystal structure of the MOF using a X'PERT diffractometer with X'Celerator detector (X'Pert Pro PANalytical) instrument using Cu Kα radiation (λ = 0.15406 nm). The thermogravimetric analysis (TGA) was used to determine the MOF stability and the amount of surfactant incorporated as well as the efficiency in the elimination process. TGAs were run from 25 to 900 °C at 20 °C min^{-1} with Perkin-Elmer TGA7 instrument under air flow. Transmission electron microscopy (TEM) micrographs were taken using a JEOL 2100F electron microscope operating at 200 kV. The samples were prepared by suspending a small amount of solid in ethanol. A drop of this suspension was then dispersed onto a holey carbon film on a copper grid, followed by drying at room temperature. Scanning electron microscopy (SEM) micrographs were collected with a Hitachi Tabletop microscope without coating.

3. Results and discussion

Starting from NH_2-MIL-53(Al), it can be deduced from the XRD profiles in Fig. 1A that the presence of F127 in the synthesis has not altered the structure of the MOF. Interestingly, increasing molar ratio of F127/$AlCl_3{\cdot}6H_2O$ seems to modify the distribution of peaks intensities in the lowest angle diffraction peaks. In the parent A0 and for AF0.005 sample the XRD profile shows similar intensity for the peaks at 2θ = 9.2° and 10° corresponding to (110) and (200) reflections respectively [28]. For AF0.01 and AF0.025, the intensity of (110) increased while the intensity of (200) decreased compared to the parent MOF (A0). This indicates the preferential crystal growth along the (110) face in the surfactant templated MOF which can change the crystal anisotropy. Fig. 1B shows the XRD patterns of the MIL-100(Fe) series using F127, those corresponding to P123 are shown in Fig. 1SA as they reproduce the same pattern. The crystalline structure of MIL-100(Fe) is not affected by the presence of F127 and P123, however sharp intensity decrease was observed in the presence of surfactants in low angle reflections more for FP0.1 compared to FF0.1 (see inset in Fig. 1B). The low angle reflections (111), (200) and (311) are related to the mesocage structure of MIL-100 (Fe) [14,38]. According to Mahugo et al., the intensity decrease is observed when the mesocage is filled with bulky species or when there is structural transformation [38]. In this particular case, since sharp decrease is observed for FP0.1 sample for all low angle reflections, it

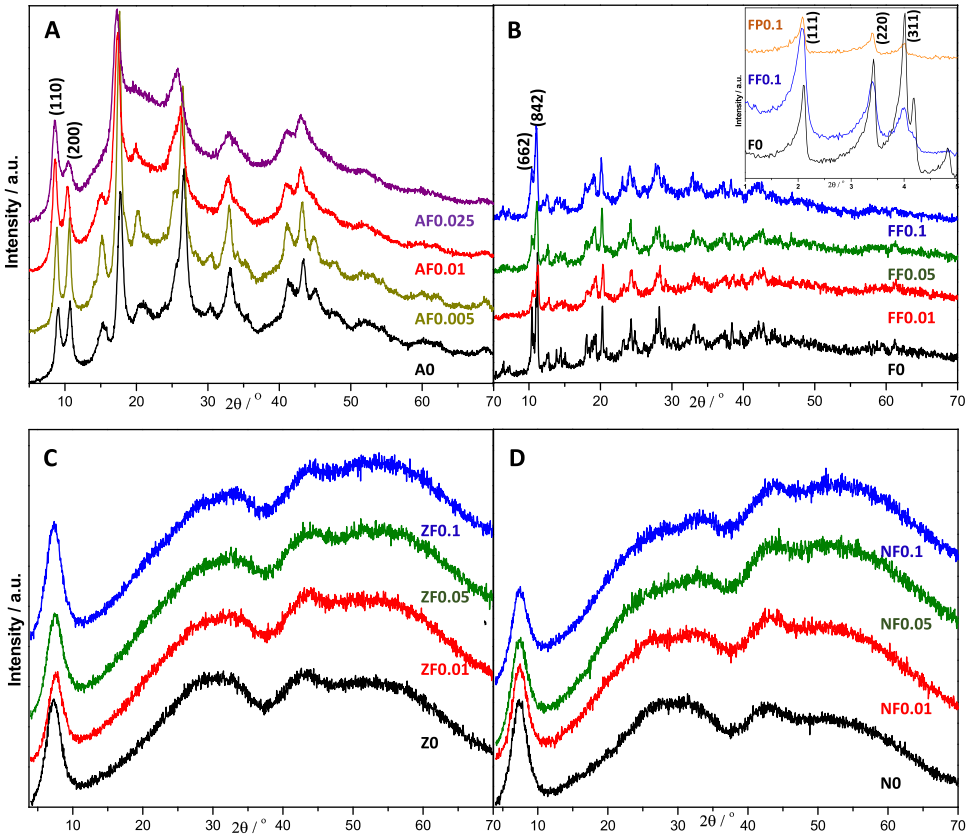

Fig. 1. XRD profiles of (A) NH_2-MIL-53(Al) (A0) and with increasing molar ratio of F127/Al source (AF0.005, AF0.01, AF0.025); (B) MIL-100(Fe) (F0) and with increasing molar ratio of F127/Fe source (FF0.01, FF0.05, FF0.01); the inset shows low angle XRD patterns of F0, FF0.1, FP0.1; (C) Zr-BDC (Z0) and with F127 (ZP0.01, ZP0.05, ZP0.1); (D) NH_2-Zr-BDC (N0) and with F127 (NP0.01, NP0.05, NP0.1).

may be attributed to the presence of P123 surfactant molecules filling the pores of the mesocages. On the other hand, F127 surfactant is very bulky and may not be able to fit in the pores of the mesocage as there is no intensity decrease observed for the (111) reflection of MIL-100(Fe) structure [39]. The high angle XRD diffraction patterns of surfactant synthesized MIL-100(Fe) for both F127 and P123 show increasing intensity in $2\theta = 11.16°$ which correspond to (842) reflections and decreasing intensity in $2\theta = 10.54°$ (662) reflection as the surfactant ratio increases [29]. This may be indicating once again certain crystal anisotropy in surfactant templated MIL-100(Fe) as compared to the parent MOF. XRD profiles in Fig. 1C correspond to Zr-BDC with F127 and in Fig. 1D for NH_2-Zr-BDC with F127. Equivalent graphs using Pluronic P123 are included in the Supplementary information to avoid repetition (Figs. 1SB and 1SC). No discernible change in the XRD profile was observed between surfactant assisted and non-assisted Zr-BDC and NH_2-Zr-BDC MOFs. The reason might be related to the semi-amorphous structure of this UiO-66 type of MOF when prepared in sustainable conditions (water and room temperature) unlike the pure crystalline phases obtained for NH_2-MIL-53(Al) and MIL-100(Fe).

TGA analyses account for the presence of surfactant and its stability upon washing. TGA curves and derivatives (DTG) are plotted for NH_2-MIL-53(Al) with F127 in Fig. 2A and for MIL-100(Fe) with F127 in Fig. 2B. Table 1 collects the weight losses of the different samples prepared with F127 surfactant with different molar ratios as well as the MOF. Table 1S collects equivalent information using Pluronic P123. There are three clearly separated weight losses: The first one due to the release of solvent, i.e. water encapsulated in the pores at approximately T < 200 °C, varying depending on the type of MOF. After that, there is the weight loss due to encapsulated linker and surfactant at a temperature range between 200 and 400 °C, and the third one corresponds to the decomposition of the structure and the release of the linker forming the MOF. Finally, at 800 °C the MOF has been completely decomposed allowing the estimation of the inorganic residue.

The first observation from the data in Tables 1 and 1S indicates that although washing with water and ethanol removed much of the surfactant, there is some amount of surfactant still present in the MOFs. The amount varies depending on molar ratio of surfactant, type of surfactant and MOF. It seems that two times ethanol washing may not be enough to remove all the surfactant present in the sample corroborating the strong interaction between the surfactant and the MOF.

For NH_2-MIL-53(Al) Fig. 2A shows how the TGA and the derivative (DTG) profiles are clearly affected by the presence of the surfactant, particularly in the range 200–400 °C where the surfactant is released together with linker in the pores of MOF [13]. For parent MOF, around 10% weight loss was observed in this temperature range due to the linker while the surfactant MOFs show 25–35% weight loss

Table 1
Weight loss calculations of synthesized MOFs with F127 surfactant.

Sample	Temperature (°C)			
	T < 220	220–400	400–800	T = 800
A0	13.59	8.87[a]	61.02	16.52
AF0.005	5.35	26.35	54.53	13.77
AF0.01	6.30	30.31	49.96	13.42
AF0.025	7.69	34.72	45.77	11.82
	T < 170	**170–300**	**300–800**	**T = 800**
F0	9.81	–	54.51	33.42
FF0.01	12.81	17.2	44.72	26.02
FF0.05	8.73	40.62	25.75	24.89
FF0.1	19.89	6.44	40.09	29.58
	T < 180	**180–400**	**400–800**	**T = 800**
Z0	11.6	–	43.94	44.46
ZF0.01	6.49	13.4	40.25	39.86
ZF0.05	6.56	16.91	38.62	37.91
ZF0.1	7.24	14.71	38.04	40.01
	T < 210	**210–400**	**400–800**	**T = 800**
N0	10	–	42.86	41.6
NF0.01	6.81	19.85[b]	40.02	33.32
NF0.05	6.34	25.19	37.27	31.2
NF0.1	5.94	22.82	39.57	31.67

[a] In this case the temperature range is 220–380 °C.
[b] In this case the temperature ranges are: T < 170; 170–300; 300–800 °C.

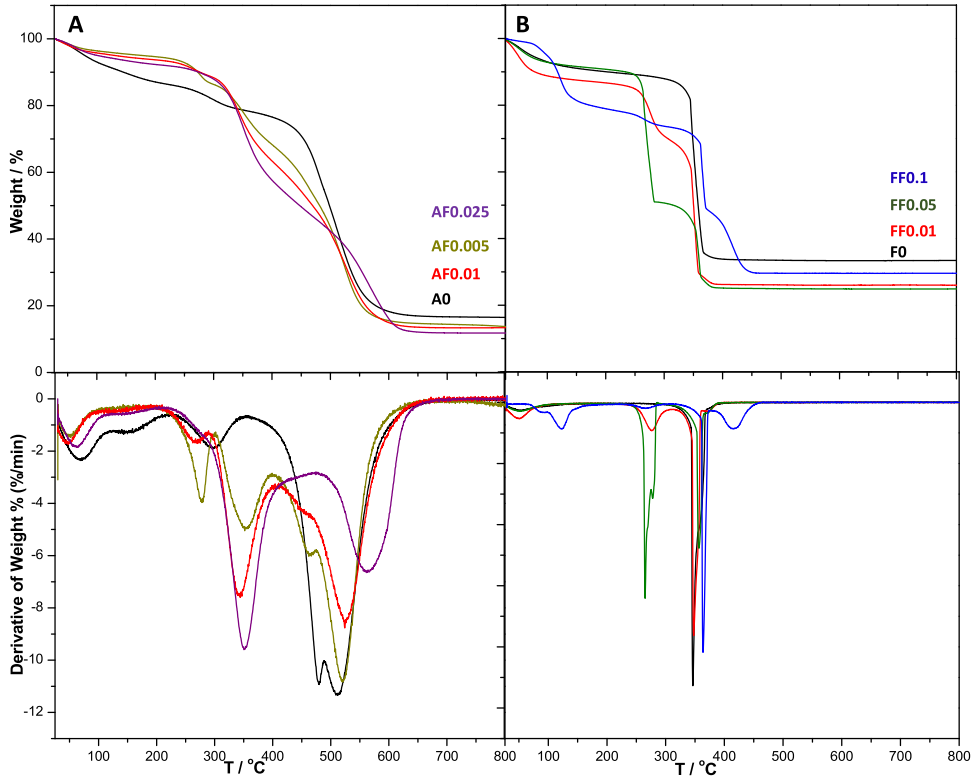

Fig. 2. Thermogravimetric analyses (top) and derivative curves (bottom) (TGA/DTG) of (A) NH_2-MIL-53(Al) F127 series, and (B) MIL-100(Fe) F127 series.

demonstrating the incorporation of the surfactant in the samples. Indeed, increasing the molar concentration of F127 surfactant in MOF synthesis increases the weight loss in the range 200–400 °C showing sharp weight loss in the derivative curves.

For MIL-100(Fe) Fig. 2B shows different curves, even with sharper derivative curves than in the previous case. Table 1 only collects the data corresponding to the F127 surfactant synthesis whereas Table 1S shows the results P123 experiments. In the first weight loss T < 170 °C there is a big difference in the F127 series: FF0.1, showed almost 20% whereas FF0.01 and FF0.05 showed less than 12% weight loss. Usually, the weight loss below 170 °C is considered as weight loss for solvent entrapped in the pores of MOFs for MIL-100(Fe) [39]. In this case, it could also be related to loosely bonded surfactant attached to the surface of the particles. In the second weight loss, any potential incorporation of the surfactant in the mesoscales of the MIL-100 structure indicated in the low angle XRD reflections should be observed. However, there is no systematic tendency in the F217 samples whereas the P123 do follow a pattern of increasing weight loss in the second temperature range as the P123 concentration increases from FP0.01 to FP0.05. The second weight loss is shifted to lower temperatures 170–300 °C as compared to the NH_2-MIL-53(Al) MOF. This may be related to the absence of NH_2-groups in this sample, or the presence of NH_2- in the NH_2-MIL-53(Al) case that may provoke stronger interactions delaying the decomposition temperature. In any case, this is mere speculation since we could not find evidences of these interactions. The third weight loss at 300–800 °C, is due to linker weight loss for parent MOF [14] and surfactant and linker weight loss together for surfactant templated MOFs. This value is more or less consistent (40–50%) in all cases except for FF0.05 that showed the lowest inorganic residue among all of them.

The TGA/DTG curves of Zr-BDC (Fig. 3A) and NH_2-Zr-BDC (Fig. 3B) are shown with surfactant F127. From the graph, it can be observed at a glance that there is a clear difference in the DTG curves in the presence of NH_2-groups although in this case, the sharp curves are observed in the absence of the amino groups rather than otherwise. In fact, the shift towards higher temperatures (stronger interactions) is observed in the NH_2-Zr-BDC system. Table 1 collects the weight losses and the temperature ranges, evidencing higher incorporation of surfactant in the NH_2-Zr-BDC system. This tendency is reproduced when the surfactant P123 is used in the synthesis gel (Table 1S).

Systematic observations by SEM were conducted in order to observe the effect of the surfactants in the final morphology and crystal size. Parent NH_2-MIL-53(Al) SEM images in Fig. 4A (A0) show large particles, yet those particles are the result of agglomerated small nanocrystals as revealed by TEM (Fig. 6A). Nevertheless, the presence of surfactant has an impact in the crystal size. The SEM micrograph for sample AF0.025 (Fig. 4B) shows presence of large crystals, as long as 235 μm, in contrast to the largest crystals measured in A0 (67 μm). This trend is observed for the presence of F127 above 0.005 $AlCl_3{\cdot}6H_2O$/F127 molar ratios as confirmed by SEM (Fig. 3S).

For MIL-100 (Fe) SEM micrographs of the parent sample (F0) show clearly agglomerates of 10–20 μm (Fig. 4C), whereas the sample prepared with surfactant F127 (FF0.1) shows perfectly formed elongated needles with an average of 60 μm long (Fig. 4D). All templated MIL-100 (Fe) synthesized with both F127 and P123 surfactant result in large crystals yet not as well formed as FF0.1 (Fig. 4S).

Fig. 5 collects SEM micrographs for UiO-66 type MOFs. Parent Zr-BDC (Z0, Fig. 5A) and NH_2-Zr-BDC (N0, Fig. 5C) show agglomerated shapeless particles grown up in large domains. The presence of surfactant shows a systematic increase in the particle size of both materials. Fig. 5B and C show as an example 0.1 F127/metal precursor molar ratio samples. Even the smallest surfactant/metal precursor molar ratios provoked the growth for both F127 and P123 surfactant as depicted in Figs. 5S and 6S. Increasing the surfactant ratios increases uniformity of the growth however not much difference was observed between 0.05 and 0.1 surfactant/metal ratios for both MOFs with F127 and P123 surfactant type.

In order to deeply investigate the directing effect of the surfactants in the MOFs crystal growth, selected samples were studied by Transmission Electron Microscopy and compared to the parent MOFs. Fig. 6 shows TEM images of NH_2-MIL-53(Al), A0 (Fig. 6A) and AF0.01 (Fig. 6B). The

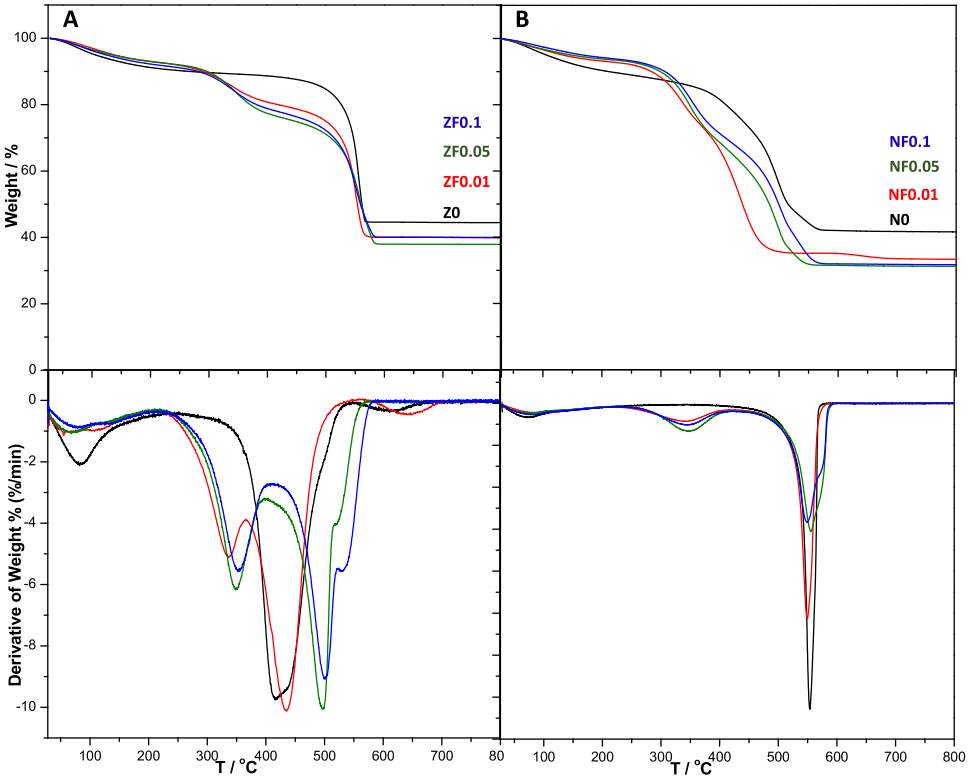

Fig. 3. Thermogravimetric analyses (top) and derivative curves (bottom) (TGA/DTG) of (A) Zr-BDC F127 series, and (B) NH_2-Zr-BDC F127 series.

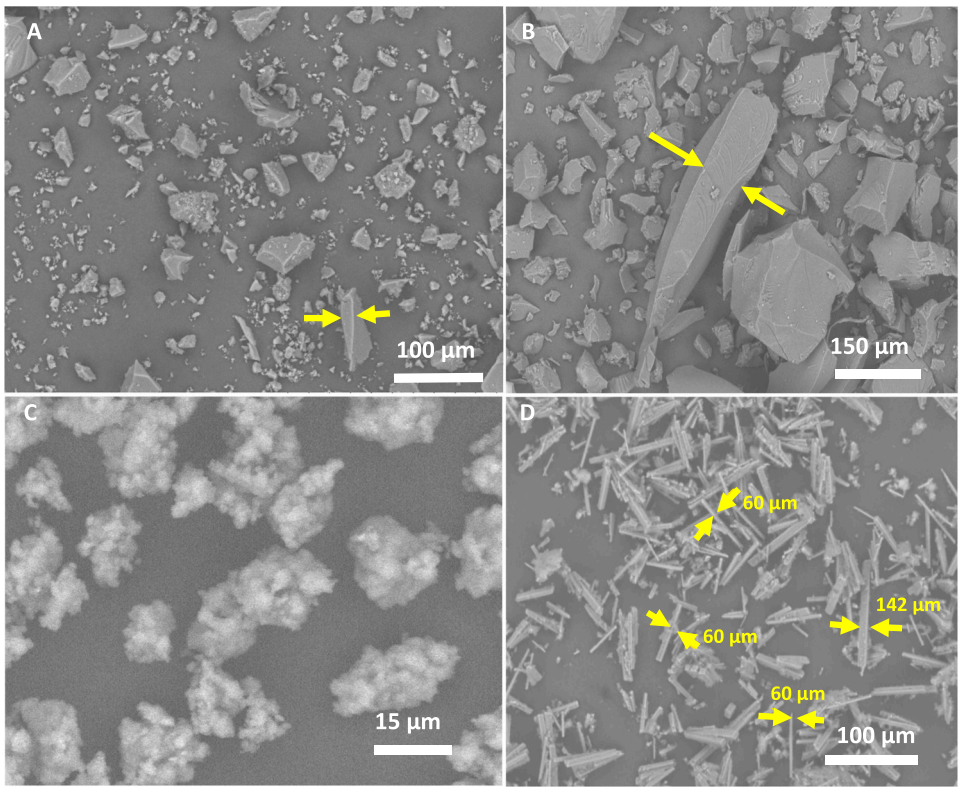

Fig. 4. SEM micrographs A) NH_2-MIL-53(Al) (A0), B) NH_2-MIL-53(Al) with 0.025 F127 (AF0.025) C) MIL-100(Fe) (F0) and D) MIL-100(Fe) with 0.1 F127 (FF0.1).

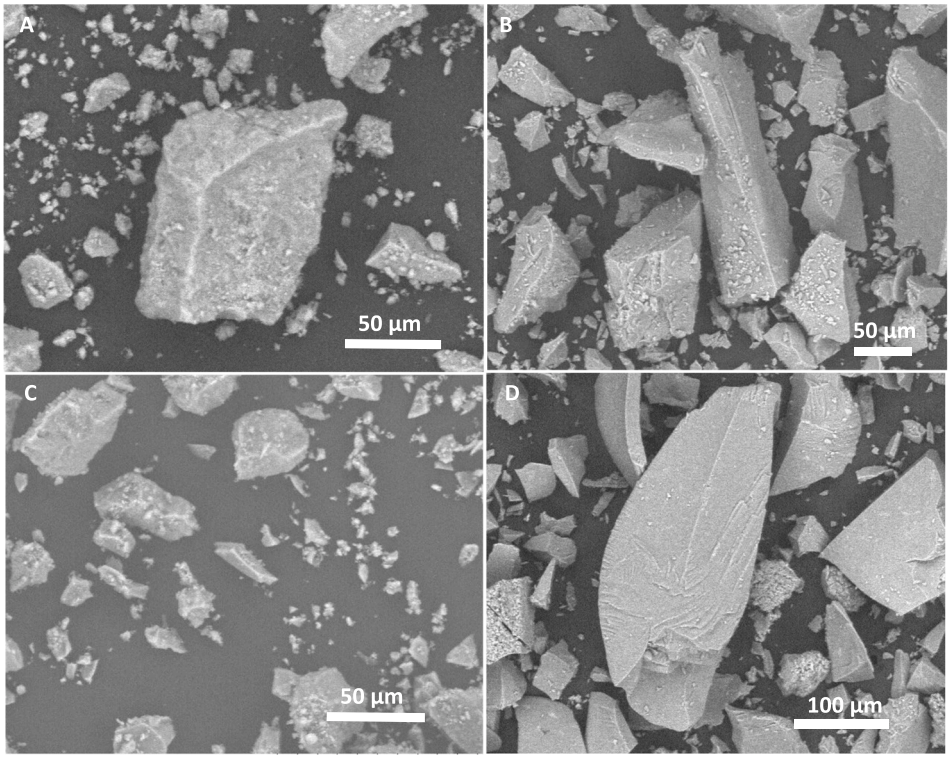

Fig. 5. SEM image of A) Zr-BDC (Z0), B) Zr-BDC with 0.1 F127 (ZF0.01) C) NH_2-Zr-BDC (N0) and D) NH_2-Zr-BDC with 0.1 F127 (NF0.01).

parent MOF is formed by agglomerated small crystals whereas the sample prepared with surfactant shows larger smoother crystals yet with no defined shape. The crystals forming MIL-100(Fe) show random particle sizes with the presence of sparsely distributed clean surfaces (Fig. 6C). In Fig. 6D, sample FF0.01 shows how the presence of surfactant has led to well-formed crystals with sharp surfaces marked by arrows in the image. These facetted crystals corroborate the XRD changes in intensity that suggested anisotropic crystals growth.

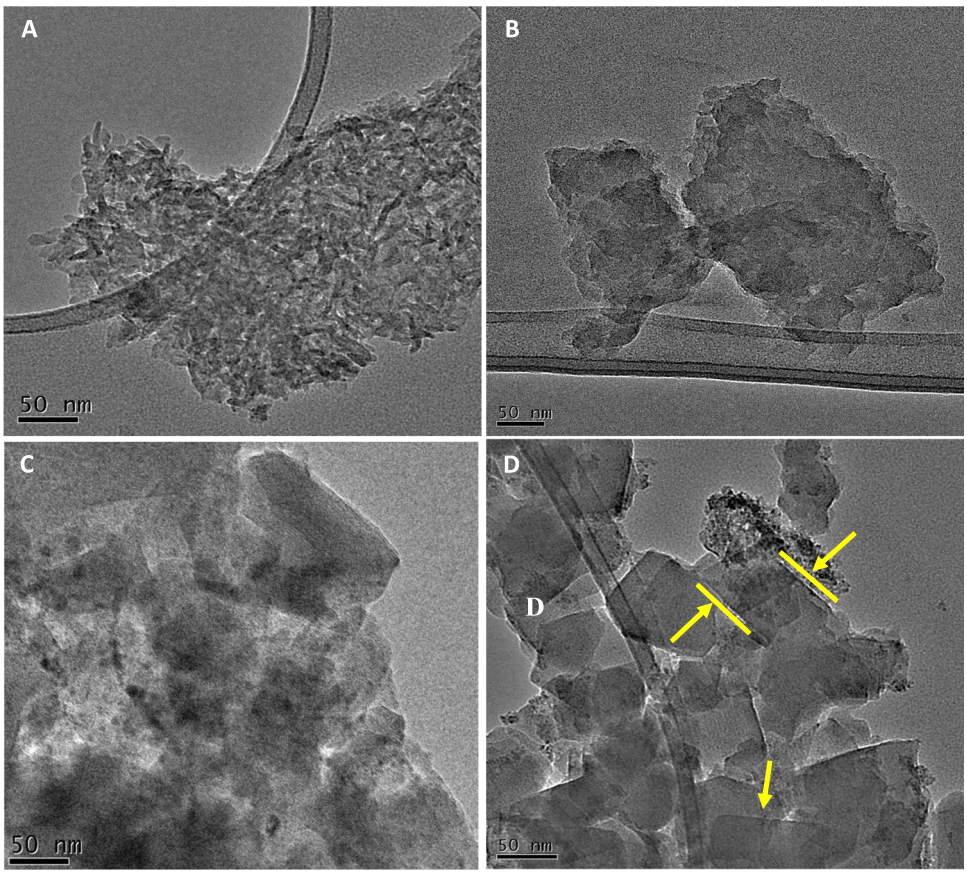

Fig. 6. TEM images of A) NH_2-MIL-53(Al) (A0), B) NH_2-MIL-53(Al) with 0.01 F127 (AF0.01) C) MIL-100(Fe) (F0) and D) MIL-100(Fe) with 0.01 F127 (FF0.01).

The effect of surfactant on Zr-BDC and NH_2-Zr-BDC is also studied by TEM. The TEM image of the parent MOF, Z0 in Fig. 7A, shows aggregates forming lager particles. The presence of F127 templated Zr-BDC, ZF0.01 in Fig. 7B, produced smooth large sized particles with different shape evidencing the effect of the surfactant in the synthesis gel. Fig. 7C and D shows the NH_2-Zr-BDC parent MOF N0 and NF0.01, respectively. The effect is exactly the same in this system, revealing how the small agglomerated particles of the parent MOF turn into smooth large particles in the surfactant assisted MOF.

From all the above described studies, it is proven that the role of the non-ionic surfactant in these MOF systems, synthesized at room temperature and water as solvent, works by aligning the MOF precursor probably via weak interactions promoting the crystal growth to form large crystals. It is known that, F127 is more hydrophilic than P123 with 106 units of ethylene oxide (EO)x ($EO_{106}PO_{70}EO_{106}$) against 20 units of ethylene oxide in P123 ($EO_{20}PO_{70}EO_{20}$). Our findings described indicate similar effect on the MOFs observed for both surfactants though the more hydrophilic nature of F127 might play a role in aligning the cationic metal precursors creating a more pronounced effect compared to P123. The F127 surfactant formed well shaped crystals grown in form of needles for MIL-100(Fe) sample. MIL-100(Fe) does not form instantaneous precipitates at room temperature synthesis. The precipitation started to form after 6 h as described in Section 2. This may give a possibility for the surfactant F127 to arrange the MOF precursors in nucleation steps. The similar effect is explained for Cu-BTC MOF with non-ionic surfactant F127, polyvinyl pyrrolidone (PVP) [25,27] and with amphoteric surfactant cocamidopropyl betaine (CAPB) [23]. The result is very noticeable crystal growth compared to the parent MOFs specifically when higher (0.1 F127/$FeCl_2{\cdot}4H_2O$) molar ratios were used. The possible scheme for the templating effect of F127 surfactant is depicted in Fig. 8 for MIL-100 (Fe). It explains how the F127 surfactant aligns the MOF precursor during nucleation stages and creates anisotropic crystal growth comparing with the synthesis of MIL-100(Fe) without the surfactant.

Fig. 9 shows the scheme for templating effect of F127 surfactant for NH_2-MIL-53(Al), Zr-BDC and NH_2-Zr-BDC MOFs. Unlike MIL-100(Fe), NH_2-MIL-53(Al), Zr-BDC and NH_2-Zr-BDC MOFs forms instantaneous precipitates when the precursor materials are mixed together as described in the synthesis section. Fig. 9 depicts the formation of agglomerated crystal during room temperature synthesis of MOFs using water as a solvent in contrast to the formation of well aligned agglomerated crystal when the reaction system is assisted with F127 surfactant. For both Figs. 8 and 9 schemes, the surfactant is presented as planar to show the effect of surfactant on directional growth of MOF.

In Fig. 10, an example is considered to show the directional crystal growth of surfactant templated MOFs taking MIL-100(Fe) structure from CIF file, CCDC 640536 [40]. The explanation taken into account suggested the directional crystal growth of the surfactant templated MOF along *b* axis perpendicular to *a* and *c* axis as exhibited in Fig. 10. The intensity of (842) plane is somehow unchanged compared to the parent MOF, however for (662) the intensity decreased indicating higher electron density distribution in the (842) plane for surfactant templated MIL-100(Fe). This structural crystal growth explains the observations obtained by SEM and TEM.

4. Conclusions

Templating effect of non-ionic surfactant on crystal size and morphology was observed for NH_2-MIL-53(Al), MIL-100(Fe), Zr-BDC and NH_2-Zr-BDC under sustainable synthesis method. The template effect of the surfactant was seen from XRD, SEM and TEM for the crystalline MOFs NH_2-MIL-53(Al) and MIL-100(Fe). For semi-amorphous type Zr-BDC and NH_2-Zr-BDC MOFs, XRD does not show differences between parent and templated MOFs. SEM and TEM characterization

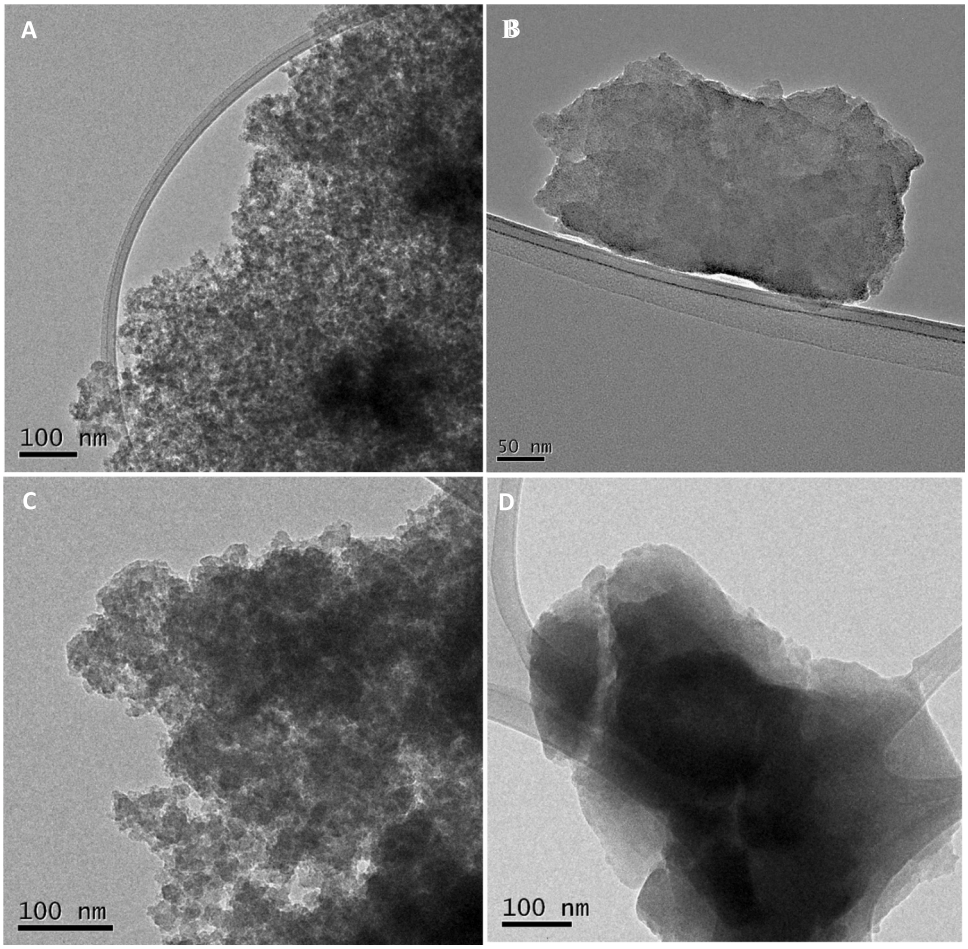

Fig. 7. TEM images of A) Zr-BDC (Z0), B) C) Zr-BDC with 0.1 F127 (ZF0.01), C) NH_2-Zr-BDC (N0) and D) NH_2-Zr-BDC with 0.1 F127 (NF0.01).

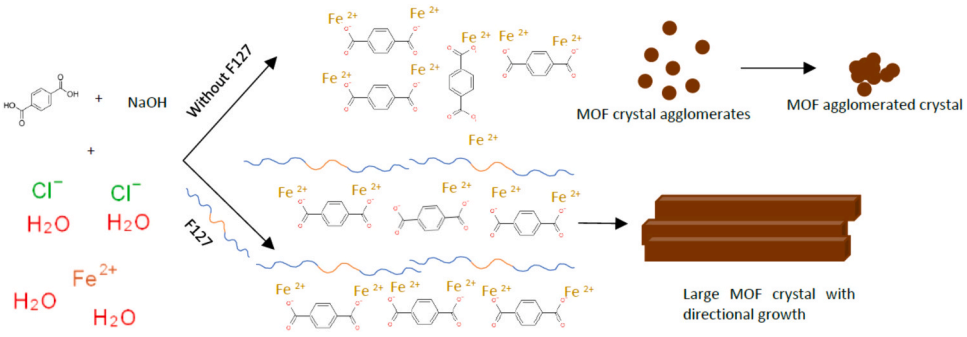

Fig. 8. Suggested process of crystal growth in the room temperature synthesized MIL-100(Fe) with and without F127 surfactant.

was used to confirm the size effect for those MOFs. In our experiments, room temperature synthesized MOFs with water as solvent without surfactant occurs with fast nucleation and with nanocrystalline aggregates. However, the presence of non-ionic surfactants in the same synthesis slows down nucleation and forms large MOF crystals. The molar ratios of surfactant to the metal precursor of the MOF greatly affect the corresponding MOF morphology as well as crystal size. For all synthesized MOFs, increasing molar ratios of surfactant/metal precursor above 0.01, created larger crystals. Large crystal size with different morphology than the parent MOF was obtained for $AlCl_3{\cdot}6H_2O$/F127, 0.025 and $FeCl_2{\cdot}4H_2O$/F127, 0.1 molar ratios. From the experiments that have been conducted, it can be concluded that the addition of surfactants enhances crystal growth of MOF at room temperature.

CRediT authorship contribution statement

All authors have read and agree to the published version of the manuscript. **Nejat Redwan Habib:** Investigation, Writing – original draft, Writing – review & editing. **Raquel Sainz:** Investigation. **Abi M. Taddesse:** Resources, Writing – review & editing, Supervision, Funding acquisition. **Isabel Diaz:** Conceptualization, Resources, Writing – original draft, Writing – review & editing, Supervision, Funding acquisition.

Declaration of Competing Interest

The authors declare that they have no known competing financial interests or personal relationships that could have appeared to influence

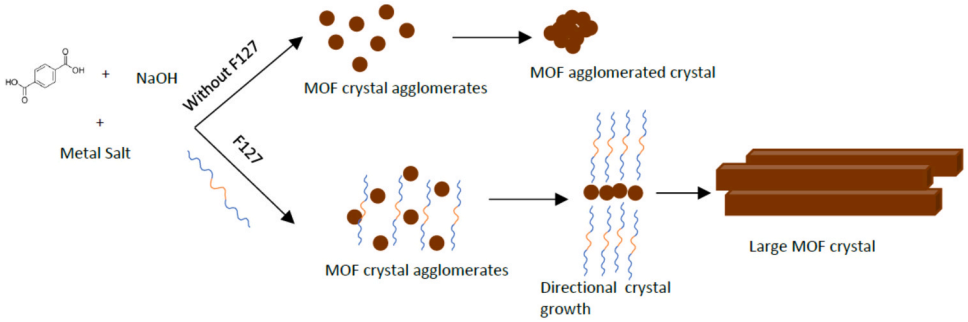

Fig. 9. General scheme for the precipitation processes in NH_2-MIL-53 (Al), Zr-BDC and NH_2-Zr-BDC MOFs room temperature syntheses with or without F127 surfactant.

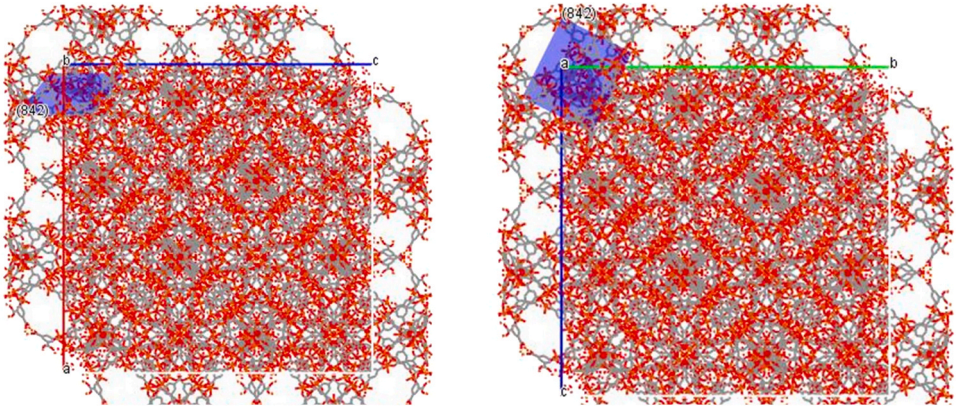

Fig. 10. One dimensional growth of surfactant assisted MIL-100(Fe) taken from CIF files.

the work reported in this paper.

Acknowledgments

Dr. Manuel Sánchez-Sánchez is acknowledged for his helpful insights in the sustainable MOF synthesis, and fruitful discussions. NRH acknowledges UNED and Fundación Mujeres por África for the scholarship Learn Africa, also Adama Science and Technology University for support. This work has been funded by CSIC Project iCOOP-2019 (COOPA20376), as well as the Spanish Agency for International Development Cooperation AECID INNOVACION (2020/ACDE/000373). Haramaya University is also acknowledged for funding via a project code HURG_2020_03_02_75.

Appendix A. Supporting information

Supplementary data associated with this article can be found in the online version at doi:10.1016/j.cattod.2021.09.028.

References

[1] H. Li, M. Eddaoudi, M. O'Keeffe, O.M. Yaghi, Design and synthesis of an exceptionally stable and highly porous metal-organic framework, Nature 402 (1999) 276–279.
[2] A.E. Baumann, D.A. Burns, B. Liu, V.S. Thoi, Metal-organic framework functionalization and design strategies for advanced electrochemical energy storage devices, Commun. Chem. 2 (2019), 86.
[3] V.V. Butova, M.A. Soldatov, A.A. Guda, K.A. Lomachenko, C. Lamberti, Metal-organic frameworks: structure, properties, methods of synthesis and characterization, Russ. Chem. Rev. 85 (2016) 280–307.
[4] J. Hwang, A. Ejsmont, R. Freund, J. Goscianska, B.V.K.J. Schmidt, S. Wuttke, Controlling the morphology of metal-organic frameworks and porous carbon materials: metal oxides as primary architecture-directing agents, Chem. Soc. Rev. 49 (2020) 3348–3422.
[5] P. Horcajada, R. Gref, T. Baati, P.K. Allan, G. Maurin, P. Couvreur, G. Férey, R. E. Morris, C. Serre, Metal-organic frameworks in biomedicine, Chem. Rev. 112 (2012) 1232–1268.
[6] Q. Zheng, X. Liu, Y. Zheng, K.W.K. Yeung, Z. Cui, Y. Liang, Z. Li, S. Zhu, X. Wang, S. Wu, The recent progress on metal-organic frameworks for phototherapy, Chem. Soc. Rev. 50 (2021) 5086–5125.
[7] B. Li, J.P. Dong, Z. Zhou, R. Wang, L.Y. Wang, S.Q. Zang, Robust lanthanide metal–organic frameworks with "all-in-one" multifunction: efficient gas adsorption and separation, tunable light emission and luminescence sensing, J. Mater. Chem. C 9 (2021) 3429–3439.
[8] M. Ding, R.W. Flaig, H.-L. Jiang, O.M. Yaghi, Carbon capture and conversion using metal-organic frameworks and MOF-based materials, Chem. Soc. Rev. 48 (2019) 2783–2828.
[9] D. Yang, B.C. Gates, Catalysis by metal organic frameworks: perspective and suggestions for future research, ACS Catal. 9 (2019) 1779–1798.
[10] I.A. Ibarra, P.A. Bayliss, E. Pérez, S. Yang, A.J. Blake, H. Nowell, D.R. Allan, M. Poliakoff, M. Schröder, Near-critical water, a cleaner solvent for the synthesis of a metal–organic framework, Green Chem. 14 (2012) 117–122.
[11] N. Getachew, Y. Chebude, M. Sánchez-Sánchez, I. Diaz, Room temperature synthesis of metal organic framework MOF-2, J. Porous Mater. 21 (2014) 769–773.
[12] M. Díaz-García, A. Mayoral, I. Díaz, M. Sánchez-Sánchez, Nanoscaled M-MOF-74 materials prepared at room temperature, Cryst. Growth Des. 14 (2014) 2479–2487.
[13] M. Sánchez-Sánchez, N. Getachew, K. Díaz, M. Díaz-García, Y. Chebude, I. Díaz, Synthesis of metal–organic frameworks in water at room temperature: salts as linker sources, Green Chem. 17 (2015) 1500–1509.
[14] K. Guesh, C.A.D. Caiuby, Á. Mayoral, M. Díaz-García, I. Díaz, M. Sanchez-Sanchez, Sustainable preparation of MIL-100(Fe) and Its photocatalytic behavior in the degradation of methyl orange in water, Cryst. Growth Des. 17 (2017) 1806–1813.
[15] I. Pakamore, J. Rousseau, C. Rousseau, E. Monflier, P.Á. Szilágyi, An ambient-temperature aqueous synthesis of zirconium-based metal–organic frameworks, Green Chem. 20 (2018) 5292–5298.
[16] A. Feliczak-Guzik, Hierarchical zeolites: synthesis and catalytic properties, Microporous Mesoporous Mater. 259 (2018) 33–45.
[17] B. Szczęśniak, J. Choma, M. Jaroniec, Major advances in the development of ordered mesoporous materials, Chem. Commun. 56 (2020) 7836–7848.
[18] D. Bradshaw, S. El-Hankari, L. Lupica-Spagnolo, Supramolecular templating of hierarchically porous metal-organic frameworks, Chem. Soc. Rev. 43 (2014) 5431–5443.
[19] D. Liu, D. Zou, H. Zhu, J. Zhang, Mesoporous metal-organic frameworks: synthetic strategies and emerging applications, Small 14 (2018), 1801454.

[20] B. Seoane, A. Dikhtiarenko, A. Mayoral, C. Tellez, J. Coronas, F. Kapteijn, Metal organic framework synthesis in the presence of surfactants: towards hierarchical MOFs? CrystEngComm 17 (2015) 1693–1700.
[21] M.A. Molina, N.R. Habib, R.M. Blanco, I. Díaz, M. Sánchez-Sánchez, Catal. Today (under revision).
[22] K. Li, S. Lin, Y. Li, Q. Zhuang, J. Gu, Aqueous-phase synthesis of mesoporous Zr-Based MOFs templated by amphoteric surfactants, Angew. Chem. Int. Ed. Engl. 57 (2018) 3439–3443.
[23] L.W. Giles, S.P. Meaney, R. Prathapan, M.J. Pottage, G.P. Knowles, A.L. Chaffee, S. R. Batten, R.F. Tabor, Surfactant-controlled crystal growth of metal–organic frameworks and their nanoparticle pyrolysis products, Acta Mater. 13 (2020), 100849.
[24] H. Zhang, J. Huo, F. Li, C. Duan, H. Xi, Rapid synthesis of hierarchical porous metal–organic frameworks and the simulation of growth, Cryst. Growth Des. 18 (2018) 6661–6669.
[25] H. Li, F. Meng, S. Zhang, L. Wang, M. Li, L. Ma, W. Zhang, W. Zhang, Z. Yang, T. Wu, S. Lee, F. Huo, J. Lu, Crystal-growth-dominated fabrication of metal–organic frameworks with orderly distributed hierarchical porosity, Angew. Chem. Int. Ed. 59 (2020) 2457–2464.
[26] P. Falcaro, A.J. Hill, K.M. Nairn, J. Jasieniak, J.I. Mardel, T.J. Bastow, S.C. Mayo, M. Gimona, D. Gomez, H.J. Whitfield, R. Riccò, A. Patelli, B. Marmiroli, H. Amenitsch, T. Colson, L. Villanova, D. Buso, A new method to position and functionalize metal-organic framework crystals, Nat. Commun. 2 (2011) 237.
[27] Y. Sun, M. Amsler, S. Goedecker, A. Caravella, M. Yoshida, M. Kato, Surfactant-assisted synthesis of large Cu-BTC MOF single crystals and their potential utilization as photodetectors, CrystEngComm 21 (2019) 3948–3953.
[28] X. Cheng, A. Zhang, K. Hou, M. Liu, Y. Wang, C. Song, G. Zhang, X. Guo, Size- and morphology-controlled NH_2-MIL-53(Al) prepared in DMF–water mixed solvents, Dalton Trans. 42 (2013) 13698–13705.
[29] F. Tan, M. Liu, K. Li, Y. Wang, J. Wang, X. Guo, G. Zhang, C. Song, Facile synthesis of size-controlled MIL-100(Fe) with excellent adsorption capacity for methylene blue, Chem. Eng. J. 281 (2015) 360–367.
[30] Y. Han, M. Liu, K. Li, Y. Zuo, Y. Wei, S. Xu, G. Zhang, C. Song, Z. Zhang, X. Guo, Facile synthesis of morphology and size-controlled zirconium metal–organic framework UiO-66: the role of hydrofluoric acid in crystallization, CrystEngComm 17 (2015) 6434–6440.
[31] Y. Zhao, Q. Zhang, Y. Li, R. Zhang, G. Lu, Large-scale synthesis of monodisperse UiO-66 crystals with tunable sizes and missing linker defects via acid/base co-modulation, ACS Appl. Mater. Interfaces 9 (2017) 15079–15085.
[32] F. Martínez, G. Orcajo, D. Briones, P. Leo, G. Calleja, Catalytic advantages of NH_2-modified MIL-53(Al) materials for Knoevenagel condensation reaction, Microporous Mesoporous Mater. 246 (2017) 43–50.
[33] Y. Qi, Y. Luan, X. Peng, M. Yang, J. Hou, G. Wang, Design and synthesis of an Au@MIL-53(NH_2) catalyst for a one-pot aerobic oxidation/Knoevenagel condensation reaction, Eur. J. Inorg. Chem. 2015 (2015) 5099–5105.
[34] S. Zhang, L. Zhou, M. Chen, Amine-functionalized MIL-53(Al) with embedded ruthenium nanoparticles as a highly efficient catalyst for the hydrolytic dehydrogenation of ammonia borane, RSC Adv. 8 (2018) 12282–12291.
[35] V.R. Bakuru, S.R. Churipard, S.P. Maradur, S.B. Kalidindi, Exploring the brønsted acidity of UiO-66 (Zr, Ce, Hf) metal-organic frameworks for efficient solketal synthesis from glycerol acetalization, Dalton Trans. 48 (2019) 843–847.
[36] M.R. DeStefano, T. Islamoglu, S.J. Garibay, J.T. Hupp, O.K. Farha, Room-temperature synthesis of UiO-66 and thermal modulation of densities of defect sites, Chem. Mater. 29 (2017) 1357–1361.
[37] M. Kalaj, K.E. Prosser, S.M. Cohen, Room temperature aqueous synthesis of UiO-66 derivatives via postsynthetic exchange, Dalton Trans. 49 (2020) 8841–8845.
[38] R. Mahugo, A. Mayoral, M. Sánchez-Sánchez, I. Diaz, Observation of Ag nanoparticles in/on Ag@MIL-100(Fe) prepared through different procedures, Front. Chem. 7 (2019) 686.
[39] M. Sanchez-Sanchez, I. de Asua, D. Ruano, K. Diaz, Direct synthesis, structural features, and enhanced catalytic activity of the basolite F300-like semiamorphous Fe-BTC framework, Cryst. Growth Des. 15 (2015) 4498–4506.
[40] P. Horcajada, S. Surble, C. Serre, D. Hong, Y. Seo, J. Chang, J. Grene, Synthesis and catalytic properties of MIL-100(Fe), an iron(III) carboxylate with large pores, Chem. Commun. 100 (2007) 2820–2822.